Top quark pair production cross-section in proton-proton collisions at √s = 7 TeV

Tsiakiris, M.

Publication date
2012

Chapter 1

Theoretical Overview

"As for me, all I know is that I know nothing."

Socrates
c.469 BC - c. 399 BC

The aim of this thesis is to perform a measurement of the production cross-section of top quark-pairs ($t\bar{t}$) in proton-proton collisions. The analysis that will be presented in the next pages uses the very first data collected by the ATLAS detector at the Large Hadron Collider. In this chapter we discuss the underlying theory that is related with this measurement and we point out its most important aspects.

In section 1.1 a brief overview of the Standard Model of particle physics is given, the theory that governs most of the observed processes in the high-energy regime. Section 1.2 discusses the environment of the hadronic collisions and presents the key elements in the structure of the formula used for estimating theoretically the cross-section. Section 1.3 dives into the top quark physics sector: from production of top quarks with emphasis to $t\bar{t}$ pairs, to the decay channels of the latter. The importance of the cross-section measurement is also highlighted. Lastly, section 1.4 provides an overview of the tools that are used to describe these processes at the simulation level and which are encountered in the rest of this thesis.

1.1 The Standard Model of Particle Physics

The Standard Model is the theory that emerged during the 1960s and 1970s as the result of extensive research in the field of High-Energy Physics [17, 30, 16, 18]. Up until that point, physicists had observed a vast number of sub-atomic particles in many different experiments (the particle "zoo") but without being able to explain their nature. The Standard Model effectively put an end to this by being able to categorize the observed physics based on a few elementary particles and their interactions. The elementary particles are categorized in *fermions* and *bosons*, with the fermions being distinguished into leptons and quarks. The basis of the Standard Model is the symmetry group $SU(3)_C \times SU(2)_L \times U(1)_Y$, where the $SU(3)_C$ group describes the strong interaction and the $SU(2)_L \times U(1)_Y$ group the unified electroweak interaction.

The bosons obey the Bose-Einstein statistics [31, 32] and have integer spin. They act as the force mediators when fermions couple with them and therefore they are considered the respective force carriers. The way a particle will interact depends on its quantum properties, thus particles with an electric charge undergo electromagnetic interactions by coupling to the

photons, particles with a *color* charge interact through the strong force of which gluons are the mediators, and lastly those with a *weak isospin* interact with the weak force exchanging a weak boson ($W^{\pm}$ or Z^0). Gravity, although it is hypothesized that is mediated by the graviton, this is yet to be experimentally confirmed and is not described by the Standard Model.

The fermions obey the Fermi-Dirac statistics [33, 34] and therefore are half-integer spin particles. They are the main constituents of matter and can be generally placed into three generations. Each generation contains an *up-type* quark, a *down-type* quark, a charged lepton and its corresponding neutrino. The only difference between corresponding fermions from each generation is their mass.

Figure 1.1 shows the different elementary particles of the Standard Model together with their value of spin, electric charge and mass. The electric charge is shown in units of elementary charge (e) which is equivalent to $1.602176 \cdot 10^{-19}$ C. The mass is shown in units of GeV[1]. For each of the particles in the table, an equivalent anti-particle exists with the same properties but with opposite quantum numbers.

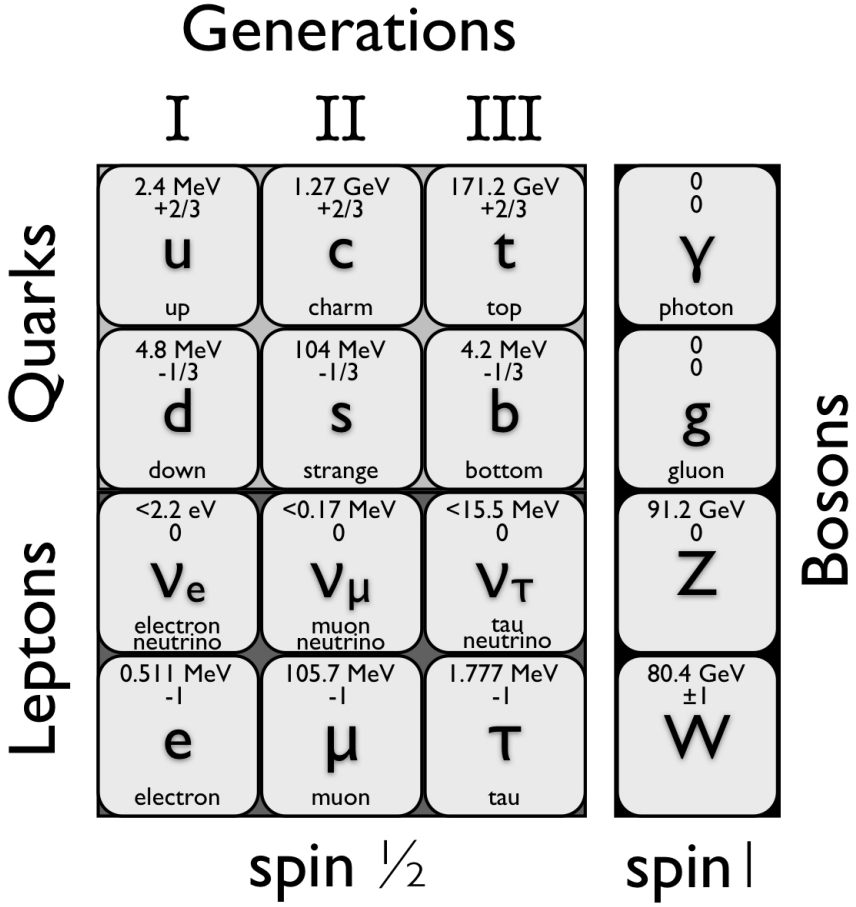

Figure 1.1: *The Standard Model elementary particles: building blocks of matter.*

[1]Throughout this thesis the natural units formalism is used, therefore $\hbar = c = 1$, where $\hbar$ is the reduced Planck constant and c is the speed of light. Consequently, momentum and mass values are given in units of eV (instead of eV/c and eV/c^2), unless stated otherwise.

1.1.1 Ingredients of the Standard Model

The Standard Model is defined as a renormalizable relativistic quantum field theory (QFT) which describes the fundamental forces of nature within a single Lagrangian. This definition laconically states a number of key ingredients which are explained in the following.

A quantum field theory

The Standard Model is a QFT, implying that the force fields that it describes are quantized. In practice, this means that a field, when "seen" at an infinite distance, can be described as a particle. Therefore, an immediate connection between the fundamental forces of nature and specific particles is established. On the other hand, it is also an approximate theory, one that is only able to describe the physics up to a certain scale. This is because there exist no widely accepted prescription with which the gravitational field can be quantized. Therefore, within the Standard Model the gravity is completely ignored and only the electromagnetic, the strong and the weak interactions are described by the Standard Model[2]!

A relativistic theory

The Standard Model is a relativistic theory, therefore it is constructed such that the laws of physics are obeyed for every inertial frame of reference. Mathematically, this means that its Lagrangian is a Lorentz scalar, namely it remains invariant under Lorentz transformations.

A renormalizable theory

Within a QFT model, calculations can be performed based on first principles by taking into account all the possible field configurations. However, this is practically impossible and therefore we rely on perturbation theory. Under perturbative calculations we can approximate the result at each order; the higher the order the better the approximation to the real value. However, by expanding to higher orders, the integrals, which generally diverge, lead to infinities. This is an unphysical result. The way that this is dealt with, is to allow the model to absorb the infinities into a finite number of physical quantities. However, an immediate consequence of this method is that the values of the relevant physical quantities may no longer be deduced from first principles. This procedure is called *renormalization* and a theory that is able to absorb all infinities without introducing new ones is called *renormalizable* [30]; the Standard Model is a renormalizable theory.

1.1.2 Symmetries

In order to understand how the fields are formulated within the Standard Model Lagrangian, one must first refer to the notion of symmetry in nature. As Emmy Noether proved in 1915, if an action remains invariant under a group of transformations, therefore implying the existence of a symmetry, then there also exist at least one conserved quantity [35, 36]. In other words, the presence of a symmetry suggests a conservation law (Noether's Theorem).

Symmetries govern the physical world, but, from them all, gauge symmetries have a special role. Gauge symmetries can be categorized in *global*, that remain constant for all space-time points, and *local* that are a function of the space-time coordinates.

[2]It should be mentioned, however, that the gravitational force is by far the weakest of all the fundamental forces. In fact, its relative strength is considered to be many orders of magnitude smaller than the other forces and therefore, in the context of particle physics, ignoring the gravitational force is entirely acceptable.

Global gauge symmetries

As the Noether Theorem suggests, a global gauge transformation leads to a conservation principle. This can be easily demonstrated with the following example of the Lagrangian[3] of the free scalar field with mass m:

$$\mathcal{L} = |\partial^\mu \phi|^2 - m^2|\phi|^2, \tag{1.1.1}$$

which remains invariant under the global gauge transformations ($a \to$ constant):

$$\phi(x) \to e^{iq\alpha}\phi(x) \text{ and} \tag{1.1.2}$$

$$\phi^*(x) \to e^{-iq\alpha}\phi^*(x). \tag{1.1.3}$$

The immediate consequence is that the current:

$$J^\mu = iq(\phi^*\partial^\mu\phi - \phi\partial^\mu\phi^*) \tag{1.1.4}$$

is conserved ($\partial_\mu J^\mu = 0$).

Local gauge symmetries

Taking again the Lagrangian in equation 1.1.1, we impose on it a local gauge transformation similar to the ones from equation 1.1.3, only that now $\alpha = \alpha(x)$. This results to the following:

$$\partial_\mu(\alpha(x)\phi) \neq \alpha(x)(\partial_\mu\phi),$$

which implies that the Lagrangian does not remain invariant. In order to save the invariance we introduce the covariant derivate:

$$D_\mu = \partial_\mu - iqA_\mu(x), \tag{1.1.5}$$

where $A_\mu(x)$ is a vector field, the *gauge field*. By requiring that the gauge field also transforms at the same time:

$$A_\mu(x) \to A_\mu(x) - \partial_\mu\alpha(x), \tag{1.1.6}$$

then the derivative of the ϕ field will give:

$$D_\mu\phi \to e^{iq\alpha(x)}D_\mu\phi \text{ and} \tag{1.1.7}$$

$$D_\mu\phi^* \to e^{-iq\alpha(x)}D_\mu\phi^* \ . \tag{1.1.8}$$

This formulation leads to the following Lagrangian which is invariant under the local gauge transformations:

$$\mathcal{L} = |\partial^\mu\phi|^2 - m^2|\phi|^2 - qJ^\mu A_\mu + q^2 A_\mu A^\mu\phi^*\phi - \frac{1}{4}F_{\mu\nu}F^{\mu\nu} \ , \tag{1.1.9}$$

where $F^{\mu\nu} = \partial^\mu A^\nu - \partial^\nu A^\mu$ is called the field strength tensor. It is evident that the first two terms in equation 1.1.9 represent the initial Lagrangian that was invariant under global gauge transformations. The next two terms represent the interaction of the scalar field ϕ with the gauge field A_μ by coupling of the latter to the current J_μ of the former. Lastly, the final term is added explicitly and it represents the contribution of the gauge field to the Lagrangian. It is introduced so that the choice of A_μ remains physical and not entirely arbitrary and it is derived such that the final Lagrangian remains invariant.

The conclusion from this exercise is that in order to have a theory which remains invariant under a local gauge transformation, an extra field is introduced. This extra field, when quantized, becomes the force carrier (gauge boson) that describes the interaction between the matter fields. All fundamental fields that are described by the SM are local gauge invariant.

[3] We refer to the Lagrangian density as the 'Lagrangian'.

1.1.3 Electroweak interactions

The electroweak interaction is built from the unification of the electromagnetic and the weak interaction and its theory was first proposed by S. L. Glashow, S. Weinberg and M. A. Salam. We define the fermionic field ψ_f which can be decomposed into a right-handed and a left-handed component based on the chirality, therefore:

$$\psi_f = \frac{1-\gamma_5}{2}\psi + \frac{1+\gamma_5}{2}\psi = \psi_L + \psi_R \ , \tag{1.1.10}$$

where γ_5 is the fifth gamma matrix of the Dirac matrices (γ^μ) and takes the value $\gamma_5 = i\gamma^0\gamma^1\gamma^2\gamma^3$, while the ψ_L and ψ_R are the left-handed and right-handed projections respectively. Left-handed fermions transform under both the $SU(2)_L$ and $U(1)_Y$ and are represented as weak-isospin doublets:

$$\psi_i = \begin{pmatrix} u_i \\ d_i \end{pmatrix} \text{ or } \begin{pmatrix} \nu_i \\ \ell_i \end{pmatrix} \ , \tag{1.1.11}$$

while right-handed fermions only transform under $U(1)_Y$ and are represented as weak-isospin singlets.

By imposing these symmetries to the Lagrangian of the free fermionic field that describes the spin-1/2 particles ψ_f (Dirac equation):

$$\mathcal{L} = i\sum_f \overline{\psi}_f \gamma_\mu \partial^\mu \psi_f \ , \tag{1.1.12}$$

the covariant derivative must take the following form in order to retain the invariance:

$$D^\mu = \partial^\mu + \frac{1}{2}ig\tau^i W_i^\mu + \frac{1}{2}ig'YB^\mu \ , \tag{1.1.13}$$

where g and g' are coupling constants, τ^i are the Pauli matrices, generators of the $SU(2)_L$, Y is the hypercharge, generator of the $U(1)_Y$, and W_i^μ $(i = 1, 2, 3)$ and B^μ are the vector fields that are introduced respectively for each symmetry group. The conserved quantities for the $SU(2)_L$ and the $U(1)_Y$ are the third component of the weak isospin (T_3) and the hypercharge respectively. They are connected via the Gell-Mann - Nishijima formula:

$$Q = T_3 + \frac{Y}{2} \ , \tag{1.1.14}$$

where Q is the conserved quantity (electric charge) of the original $U(1)_{EM}$ symmetry group that describes quantum electrodynamics (QED). As before, the vector fields that are introduced by each group must also be transformed:

$$B^\mu = B^\mu - \partial^\mu \alpha(x) \ , \tag{1.1.15}$$

$$W_i^\mu = W_i^\mu - \partial^\mu \beta_i(x) - g\varepsilon_{ijk}\beta_j(x)W_k^\mu \ , \tag{1.1.16}$$

where ε_{ijk} is the Levi-Civita symbol, and the $\alpha(x)$ and $\beta_j(x)$ are phases. In the end the electroweak Lagrangian consists of the following terms:

$$\mathcal{L} = \mathcal{L}_{fermion} + \mathcal{L}_{interaction} + \mathcal{L}_{gauge} \ , \tag{1.1.17}$$

where:

$$\mathcal{L}_{fermion} = i\sum_f \overline{\psi}_f \gamma_\mu \partial^\mu \psi_f = i\overline{L}\gamma^\mu \partial_\mu L + i\overline{R}\gamma^\mu \partial_\mu R \ , \tag{1.1.18}$$

$$\mathcal{L}_{interaction} = \overline{L}\gamma^\mu(-\frac{g}{2}\tau^i W_\mu^i - \frac{g'}{2}YB_\mu)L + \overline{R}\gamma^\mu(-\frac{g'}{2}YB_\mu)R \ , \tag{1.1.19}$$

$$\mathcal{L}_{gauge} = -\frac{1}{4}W_{\mu\nu}^i W^{i,\mu\nu} - \frac{1}{4}B_{\mu\nu}B^{\mu\nu} \ . \tag{1.1.20}$$

The parameters L and R denote the left-handed doublets and right-handed singlets for the fermions, while the $W^i_{\mu\nu}$ and $B_{\mu\nu}$ correspond to the field strength tensors. Similarly to the example showed in section 1.1.2, the first term corresponds to the fermion field with its left-handed and right-handed components, the second term represents the interaction of the fermions with the gauge bosons, and the last term provides the contribution and self-interactions of the vector fields. Rewriting the interaction term, we can separate it into two categories:

$$\mathcal{L}_{charged} = -\frac{g}{2}\overline{L}\gamma^\mu(\tau^1 W^1_\mu + \tau^2 W^2_\mu)L \text{ and} \tag{1.1.21}$$

$$\mathcal{L}_{neutral} = -\frac{g}{2}\overline{L}\gamma_\mu\tau^3 W^3_\mu L - \frac{g'}{2}\overline{L}\gamma^\mu Y B_\mu L - \frac{g'}{2}\overline{R}\gamma^\mu Y B_\mu R. \tag{1.1.22}$$

$\mathcal{L}_{charged}$ evidently contains only left-handed components, therefore it can be written in the following form:

$$\mathcal{L}_{charged} = -\frac{g}{2}\overline{L}\gamma^\mu \begin{pmatrix} 0 & W^1_\mu - iW^2_\mu \\ W^1_\mu + iW^2_\mu & 0 \end{pmatrix} , \tag{1.1.23}$$

where it is possible to extract the definition of the charged gauge boson as the linear combination of the vector fields, namely:

$$W^\pm_\mu = \frac{1}{\sqrt{2}}(W^1_\mu \mp W^2_\mu). \tag{1.1.24}$$

The fact that left-handed fermions do not undergo charged current interactions is incorporated through the vector (V) and axial-vector (A) components that are introduced and is in accordance to the experimental observation of parity violating processes. Equivalently, from the $\mathcal{L}_{neutral}$, which contains both left-handed and right-handed components, we can redefine the fields in the following way:

$$\begin{pmatrix} A_\mu \\ Z_\mu \end{pmatrix} = \begin{pmatrix} \cos\theta_W & \sin\theta_W \\ -\sin\theta_W & \cos\theta_W \end{pmatrix} \begin{pmatrix} B_\mu \\ W^3_\mu \end{pmatrix} , \tag{1.1.25}$$

which gives the neutral gauge bosons as a combination of the introduced vector fields. The parameter θ_W is called the Weinberg angle and it relates with the coupling constants in the following way:

$$\sin\theta_W = \frac{g'}{\sqrt{g^2 + g'^2}} , \tag{1.1.26}$$

$$\cos\theta_W = \frac{g}{\sqrt{g^2 + g'^2}} . \tag{1.1.27}$$

In conclusion, the introduced vector fields which are required to retain the invariance of the electroweak Lagrangian, give rise to gauge bosons that act as mediators of the electroweak interaction. However, in the initial formalism these gauge bosons are expected to be massless. This contradicts the experimental observations since the $W^\pm$ and Z^0 have a mass. If those masses are put in by hand then the invariance of the Lagrangian breaks. As a result, an additional mechanism is required.

1.1.4 The Higgs mechanism

The Higgs mechanism [19, 20, 21] is the proposed theory with which the mass of the gauge bosons, evident in the weak interactions, is explained. The theory suggests to introduce a

complex scalar field doublet:

$$\phi = \begin{pmatrix} \phi^+ \\ \phi^0 \end{pmatrix} , \tag{1.1.28}$$

which remains invariant under $SU(2)_L$ transformations. We write the Lagrangian of the system:

$$\mathcal{L}_{Higgs} = (D_\mu \phi)^\dagger (D^\mu \phi) - V(\phi) , \tag{1.1.29}$$

where $V(\phi)$ is the potential of the field (Higgs potential) and is given by:

$$V(\phi) = -\mu^2 |\phi|^2 + \lambda^2 |\phi|^4. \tag{1.1.30}$$

The covariant derivative in the Lagrangian is also chosen such that it remains invariant under the $SU(2)_L \times U(1)_Y$ transformations. In the notation in equation 1.1.30, λ is a positive constant, while μ^2 denotes the mass term of the field. When $\mu^2 > 0$, the Lagrangian transforms to the QED equivalent of a charged scalar particle with mass μ and ϕ^4 self-interactions. However, if $\mu^2 < 0$ then the minimum of the potential is given by:

$$|\phi_0|^2 = -\frac{\mu^2}{2\lambda} \tag{1.1.31}$$

and not zero as one might have expected. This value, referred to as the vacuum expectation value, defines in fact a circle of minima and therefore an infinite number of ground states for the Higgs potential. We can choose an arbitrary value without loss of generality:

$$\phi_0 = \begin{pmatrix} 0 \\ u/\sqrt{2} \end{pmatrix} , \tag{1.1.32}$$

where $u = \sqrt{-\mu^2/\lambda}$. This, however, breaks the invariance under $SU(2)_L \times U(1)_Y$ transformations (spontaneous symmetry breaking) but retains it for the $U(1)_{EM}$ symmetry group. By perturbing the system and by an appropriate choice of gauge, we can write:

$$\phi(x) = \frac{1}{\sqrt{2}} \begin{pmatrix} 0 \\ u + h(x) \end{pmatrix} , \tag{1.1.33}$$

and the Lagrangian now becomes:

$$\begin{aligned} \mathcal{L}_{Higgs} = & \frac{1}{8} \left[g^2 (W_1^2 + W_2^2) + (-g W_3 + g' Y B_\mu)^2 \right] (u + h(x))^2 \\ & + \frac{1}{2} (\partial h(x))^2 - \mu^2 (h(x))^2 - u\lambda (h(x))^3 - \frac{1}{4} \lambda (h(x))^4 , \end{aligned} \tag{1.1.34}$$

where, using the equations 1.1.23 and 1.1.25, the first two terms can be written as:

$$\mathcal{L}_{Higgs} = \frac{1}{2} g^2 W^+ W^- (u + h(x))^2 + \frac{1}{8} (g^2 + g'^2) Z^2 (u + h(x))^2 + 0 \cdot A_\mu^2 + \dots \tag{1.1.35}$$

Evidently, under this formulation mass terms have been included in the Lagrangian and consequently in the Standard Model; they are given by:

$$M_W = \frac{1}{2} u g \text{ and} \tag{1.1.36}$$

$$M_Z = \frac{1}{2} u \sqrt{g^2 + g'^2} , \tag{1.1.37}$$

while for gauge field A_μ the mass term is zero, pointing to the massless photon. The vacuum expectation value (u) is approximated to $u \approx 246$ GeV and the theoretically expected values of the W and Z bosons are in good agreement with the experimental results.

The emergence of these masses comes as a result of the Goldstone theorem. Once the symmetry was broken, due to the choice of a ground state value for the potential, three massless bosons appear (Goldstone's theorem). These are subsequently absorbed by the gauge fields as their longitudinal polarization, hence giving a mass to the gauge bosons. The massless field (photon), that still remains, preserves the $U(1)_{EM}$ symmetry. From the initial four degrees of freedom of the Higgs doublet, however, one more remains and it corresponds to the physical Higgs field, which has a mass term provided by:

$$M_{Higgs} = \sqrt{2\lambda u} \ . \tag{1.1.38}$$

This is the so-called Higgs boson. Since the λ parameter is entirely arbitrary, there is no prediction on the expected mass of this particle and thus it can only be probed experimentally. Discovering this new particle, which is well motivated by the theory, is one of the major goals of the physics program of the Large Hadron Collider.

Yukawa interactions

The Higgs mechanism, as presented so far, does not offer an answer on the mass of the fermions. In fact, in the Lagrangian the fermions remain massless contradicting the experimental observations. To tackle this problem an extra term is introduced which allows the fermions to interact with the Higgs field; the Yukawa interaction. The Lagrangian term is of the form:

$$\mathcal{L} = -\lambda_f \overline{L}\phi R - \lambda_f \overline{R}\phi^\dagger L \ , \tag{1.1.39}$$

where λ_f is the coupling between the fermion and the Higgs field. As before, when the symmetry breaks, the fermions acquire mass which is given by:

$$M_f = \frac{\lambda_f}{\sqrt{2}} u \ . \tag{1.1.40}$$

Like for the case of the Higgs boson, the parameter λ_f is not predicted by the theory and as a result it can only be probed experimentally.

1.1.5 Strong interactions

The description of the strong interactions arises from the need to explain why quarks form mesons ($q\overline{q}$) and baryons (qqq or $\overline{qqq}$). A particularly interesting example is the pion-proton resonance Δ^{++}, which consists of three up-quarks (uuu) thus having the following quantum numbers: charge $Q = 2$ and isospin $I = 3/2$. The resonance with the known terms is symmetric under permutation of two quarks, something that contradicts the Pauli principle; no two identical fermions (half-integer spin particles) are allowed to occupy the same quantum state simultaneously. To accommodate the reasoning of Pauli the notion of *color* charge was introduced by O. W. Greenberg in 1965, an arbitrary quantum number that leaves the state antisymmetric. The values of the color charge are *red, blue* and *green*. Under this definition all hadrons are color-neutral, with the baryons carrying all three colors and the mesons, which are made from a quark-antiquark pair, carrying a color and its complimentary color (anti-color) charge.

The symmetry group $SU(3)_C$ is introduced in the Standard Model in order to describe the strong interactions. The color C is the conserved quantity and the generators of the group are

given by the eight Gell-Mann matrices λ_i (3-dimensional equivalent to the Pauli matrices). The Lagrangian is given by:

$$\mathcal{L}_{QCD} = \sum_{flavors} \overline{\psi}_q (i\gamma^\mu D_\mu - m)\psi_q - \frac{1}{4} G^a_{\mu\nu} G^{a,\mu\nu} \ , \tag{1.1.41}$$

where as ψ_q are the Dirac four-spinors corresponding to the quark fields, D_μ is the covariant derivative, and $G^a_{\mu\nu}$ is the field strength tensor. The index a corresponds to the gluon-color index $a = 1, \ldots, 8$. The number of flavors in the Lagrangian runs up to six, to account for all the known quarks, while also they appear in three color charges (not shown in the notation). The covariant derivative is given by:

$$D_\mu = \partial_\mu + i g_s \lambda_a A^a_\mu \ , \tag{1.1.42}$$

where g_s corresponds to the coupling constant of the strong interaction while A^a_μ denotes the gluon fields. The field strength tensor is also given by:

$$G^a_{\mu\nu} = \partial_\mu A^a_\nu - \partial_\nu A^a_\mu - g_s f^{ABC} A^B_\mu A^C_\nu \ . \tag{1.1.43}$$

The gluons which have been referred up to this point, are naturally the carriers of the strong force. They are massless, spin-1 particles with no electric charge, no hypercharge and no isospin. However, they do hold color charge which allows them to also couple with themselves. The coupling of the strong interaction is given by the following relation:

$$\alpha_s = \frac{g_s^2}{4\pi} \ . \tag{1.1.44}$$

This coupling, however, depends on the momentum scale of the interaction, denoted as Q^2; it is a 'running coupling'. This is understood after including higher order corrections in the strong interactions. Taking into account fermion loops (virtual fermion-antifermion pairs), vacuum polarization terms are included which pronounce the effect of *screening* of the color charge[4]. However, gluon contributions have a different effect as they also have a color charge but in addition an anti-color magnetic moment. Eventually, the gluon correction acts in the opposite direction of screening (*anti-screening*). The overall effect results in a prevailing anti-screening effect. The renormalized coupling constant - where the renormalization is required in the process of higher order corrections to avoid ultraviolet divergencies - is given by:

$$\alpha_s(Q^2) = \frac{\alpha_s(\mu_r^2)}{1 + \frac{1}{12\pi}\alpha_s(\mu_r^2) \cdot (11N_C - 2N_f) \ln\left(\frac{Q^2}{\mu_r^2}\right)} \ , \tag{1.1.45}$$

where N_C is the number of color charges ($N_C = 3$) and N_f is the number of fermions and depends on the scale Q^2 ($N_f = 6$ when $Q > M_{top}$, while $N_f < 6$ for lower energies). The parameter μ_r^2 is a reference mass parameter directly related with the choice of the renormalization scale. We can introduce a mass scale Λ_{QCD}; a scale for which the strong coupling constant is infinite:

$$\ln(\Lambda^2_{QCD}) = \ln(\mu_r^2) - \frac{12\pi}{11N_C - 2N_f \alpha_s(\mu_r^2)} \ , \tag{1.1.46}$$

and the equation 1.1.45 then takes the form:

$$\alpha_s(Q^2) = \frac{12\pi}{(11N_C - 2N_f) \ln\left(\frac{Q^2}{\Lambda^2_{QCD}}\right)} \ . \tag{1.1.47}$$

[4] Analogously to QED where electron-positron pairs emerging in higher-orders act as dipoles around the real charge inducing a partial screening effect.

It is evident that when $Q^2 \to \infty$, namely the distance of the interaction shrinks, the coupling goes to zero suggesting that quarks behave as free particles. This is the *asymptotic freedom* effect and it allows us to use perturbation theory in QCD at high energies. On the other hand, it is by definition that when Q^2 is low, namely $Q^2 \to \Lambda^2_{QCD}$, the coupling goes to infinity and all perturbative computations fail. This effect describes the *color confinement* which suggests that no free quarks can be directly observed by experiments. The value of the Λ_{QCD} scale can be extracted experimentally after choosing a renormalization scheme, its value for the modified minimal subtraction scheme ($\overline{MS}$) and for $N_f = 5$ is approximately ~ 200 MeV.

1.2 Cross-section in hadronic collisions

At the LHC, proton beams are used as the colliding particles[5]. The proton is a baryon consisting of two up-quarks and one down-quark (valence quarks), each carrying a different color-charge thus forming a bound neutral-color state. In addition, gluons as well as pairs of quark-antiquarks (sea-quarks) emerge briefly due to quantum fluctuations. The interesting collisions, namely collisions where new particles appear, occur when the constituents of the two opposite-moving protons interact with each other (inelastic process). Such a process is rather complex but it can be separated into the following parts:

- The *parton*[6] *distribution function (PDF)*: when constituents of the protons interact with each other, each carries a fraction of the total momentum of the initial particle ($x \in (0, 1)$). This fraction is modeled by the PDF, which is defined as the probability density for having a particle with momentum fraction x at a given scale Q^2. Clearly, PDFs are not an inherent part of the inelastic collisions but are rather a parametrization that facilitates calculations. It should be noted that PDFs cannot be estimated with perturbative QCD and therefore are extracted from experimental data, typically involving global fits to the data of deep-inelastic scattering experiments e.g. from the HERA *ep* collider experiments H1 [37, 38, 39, 40] and ZEUS [41, 42], as well as fixed target experiments e.g. NuTeV [43], including results from Drell-Yan [44] and jet production processes [45, 46, 47] . Figure 1.2 shows an example of a PDF for two different Q^2 values. It uses the parametrization of the MSTW group, which stands for A.D. Martin, W.J. Stirling, R.S. Thorne and G. Watt. The complete list of data included in this fit can be found in [48].
- *The hard-process*: the interaction between two partons from each of the colliding protons, when it happens at sufficiently high energy, has the result to break their confinement and lead to the appearance of other particles. The products of the hard-process are usually the signature of interest.
- The *initial state radiation (ISR)*: incoming partons may radiate quarks or gluons due to quantum fluctuations, therefore losing part of the parton's initial momentum fraction.
- The *final state radiation (FSR)*: outgoing partons, similarly to what happens in the case of ISR, radiate quarks or gluons. Although, the definition between ISR and FSR is very similar, kinematically they differ substantially.
- The *underlying event*: proton remnants, namely everything but the hard-process partons, also contribute to the overall process as they hold a color charge. Usually, the underlying event manifests itself through soft scatterings. The ISR/FSR processes can also be regarded as part of the underlying event.

[5] The LHC can also collide heavy ion beams but these collisions are out of the scope of this thesis.
[6] Quarks and gluons are collectively referred to as partons.

- The *hadronization*: outgoing partons from any of the previous processes eventually form hadrons as a result of the color confinement.
- The *decay*: formed hadrons or other unstable particles that may be formed during the hard-process eventually decay into more stable particles. Oftentimes, extensive radiating effects from a single parton may lead to a spray of particles towards the same direction. This formation is typically referred to as a jet.

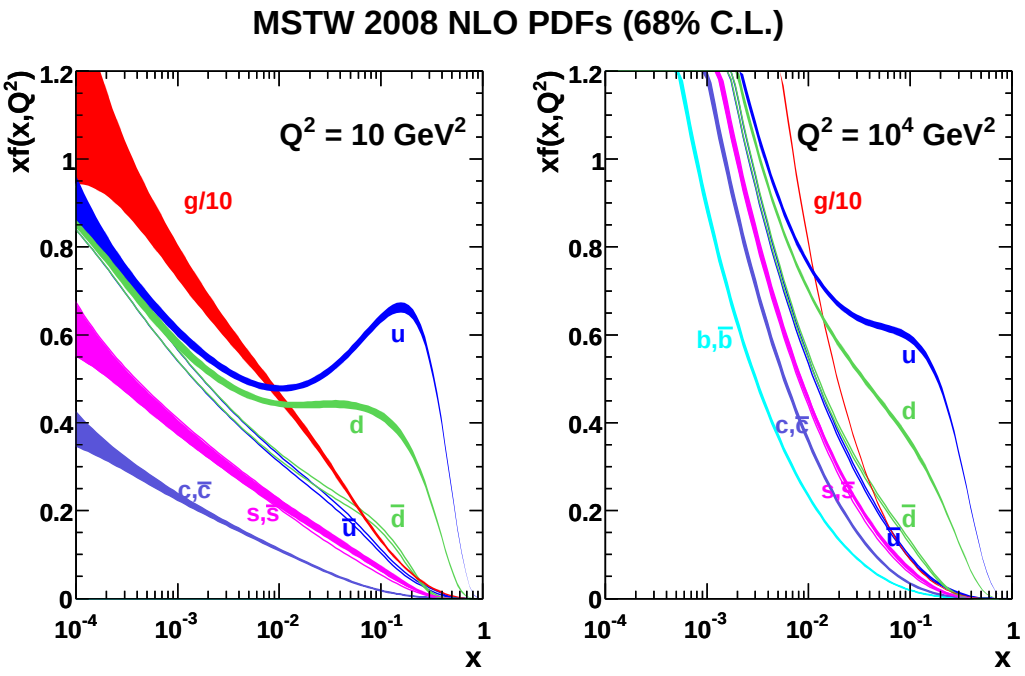

Figure 1.2: *The* `MSTW2008NLO` *PDF of protons for two different scales (Q^2) and as function of the parton momentum fraction x. The letter g is given for the gluons while u, d, s, c denote the corresponding quarks, with the anti-quarks given with as e.g. $\bar{u}$; see also figure 1.1. It should be noted that the estimate for gluons is divided by an order of magnitude, hence shown as $g/10$. Plots taken from [48].*

Calculating the cross-section of a process based on the original incoming and outgoing particles is an unfeasible task. The main reason is that we cannot have knowledge of the momentum carried by each parton since they are constituents of the proton. Instead, we calculate the cross-section at the hadronic level. Consider the process depicted in figure 1.3 where the two incoming protons have momenta P_1 and P_2 and their interacting partons have momenta that are given by $p_1 = x_1 P_1$ and $p_2 = x_2 P_1$, respectively. The hadronic cross-section is formulated as follows:

$$\sigma(P_1, P_2) = \sum_{i,j} \int dx_i dx_j f_i(x_1, \mu_f^2) f_j(x_2, \mu_f^2) \hat{\sigma}_{ij} \left(p_1, p_2, \alpha_s(\mu_r^2), \frac{Q^2}{\mu_r^2}, \mu_f^2 \right) , \tag{1.2.1}$$

where Q is the scale of interaction and the functions $f_i(x_1, \mu_f^2)$ and $f_j(x_2, \mu_f^2)$ are the corresponding PDFs at a certain *factorization scale* μ_f. The $\hat{\sigma}_{ij}$ denotes the cross-section of partons i and j at short-distance physics[7] and therefore can be calculated using perturbation theory.

[7] We refer to *short-distance* physics the regime within which we can perform perturbative calculations (due to asymptotic freedom). Likewise, long-distance physics suggests the opposite.

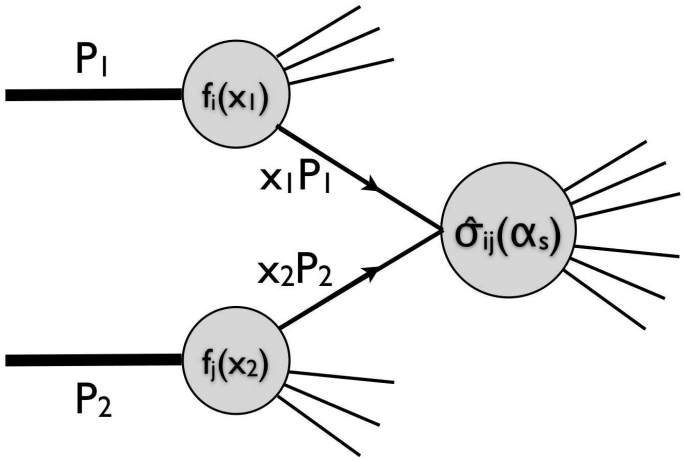

Figure 1.3: *An example of a hard-process interaction.*

Thus, it is given by:

$$\hat{\sigma} = \alpha_s^k \sum_{m=0}^{n} c_m \alpha_s^m \ , \tag{1.2.2}$$

where c_m are functions with kinematic variables and k gives the leading power of the interaction. It is important to note that with this formulation, when including higher orders, the cross-section formula may show terms which cause divergencies. These naturally break the calculation but can effectively be factored out by including them in the PDFs in equation 1.2.1; the PDFs are experimentally estimated. The factorization scale, shown above, is similar to the renormalization scale in the sense that it is pre-defined and somewhat arbitrary. It is set such that it defines the threshold between long-range and short-range physics so that a radiating parton with momentum less than the given scale becomes part of the PDF, else it contributes to the short-distance cross-section. Typically, the factorization scale and the renormalization scales are set to be equivalent to the interaction scale Q. For a calculation of the cross-section at infinite order the result is entirely independent on the chosen renormalization and factorization scales, however, as this is computationally unfeasible, a residual dependence always exists at the theoretical level that depends on the non-included higher orders.

Figure 1.4 shows the cross-section evolution for various processes in proton-antiproton (Tevatron) and proton-proton collisions (LHC) as a function of the center-of-mass energy $(\sqrt{s})$[8].

1.3 Top-quark physics

From all the particles of the Standard Model this thesis focuses on the top quark. In 1973, the existence of the top quark was implied theoretically by the prediction of M. Kobayashi and T. Maskawa on the existence of at third generation of quarks as a mean to explain CP-violation in kaon decays [22]. As their theory was heavily relying on the GIM mechanism (by S.L. Glashow, J. Iliopoulos and L. Maiani) [50] it was not until the discovery of the J/ψ meson $(c\bar{c})$ in 1974 [51, 52], which verified the existence of charm quark based on the same mechanism, that it was actually believed as a plausible theory. The prediction was further solidified with

[8]The center-of-mass energy is given by: $\sqrt{s} = \sqrt{(E_1 + E_2)^2 - (\mathbf{p}_1 + \mathbf{p}_2)^2}$, where E and $\mathbf{p}$ denote the energy and the momentum vector of the particle respectively.

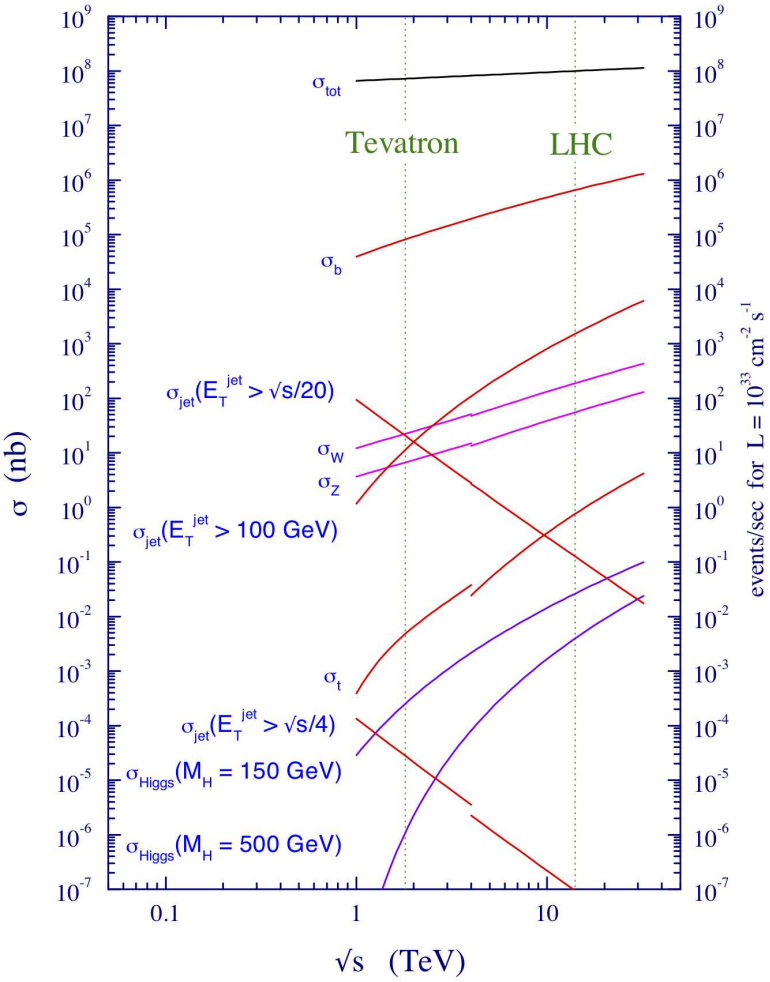

Figure 1.4: *Evolution of cross-section for proton-antiproton (Tevatron) and proton-proton (LHC) collisions. Plot taken from [49].*

the discovery of the bottom quark by the E288 experiment at Stanford's Linear Collider in 1977 [23]. Eventually, the top quark was first observed at the Tevatron proton-antiproton collider in 1995 by both the CDF [24] and DØ [25] experiments. As it stands today, it is by far the heaviest of all experimentally known elementary particles with a mass estimated at $M_t = 172.9$ GeV [53].

1.3.1 Production of top quarks in hadronic collisions

Top-quarks can be produced via both electroweak and strong interactions. In the first case, a single quark is produced. Three distinct channels exist: the Wt-channel where the top quark is produced in association with a W boson; the t-channel where a virtual W boson transforms a bottom quark into a top quark (t-channel); the s-channel where a time-like off-shell W boson decays into a top and a bottom quark.

In the second case, which is also the focus of this thesis, the top quark is produced in pairs of a top and an anti-top quark ($t\bar{t}$). It is interesting to see what is the momentum fraction threshold for the production of a $t\bar{t}$ signature. Considering the $t\bar{t}$ as a single-particle system with invariant mass $M = 2M_{top}$, we can write the rapidity of the system with the following

terms:

$$y = \frac{1}{2} \ln \frac{E + p_z}{E - p_z} \ , \tag{1.3.1}$$

with E and p_z the total energy and the longitudinal momentum of the system as measured in the lab-frame. The momentum fractions carried by the incoming partons are given by:

$$x_1 = \frac{M}{\sqrt{s}} e^{+y} \ , \text{ and} \tag{1.3.2}$$

$$x_2 = \frac{M}{\sqrt{s}} e^{-y} \ . \tag{1.3.3}$$

If $p_z = 0$, no boost is experienced in the system and the rapidity is $y = 0$. Consequently, the momentum fractions of the partons are equal, $x_1 = x_2$. For this system, we can define the threshold, x_{thr}, for each of the partons momentum fraction by simply substituting M with 346 GeV (assuming a top quark invariant mass of 173 GeV) and with $\sqrt{s}$ given by the energy of the collision. Thus, it will be $x_{thr} \sim 0.18$ and $x_{thr} \sim 0.05$ for the energies of the Tevatron (1.96 TeV) and the LHC (7 TeV) respectively. This clearly suggests that at the LHC, in comparison to the Tevatron, also partons with much lower momentum fraction will be contributing thus increasing greatly the cross-section. In addition, with the help of figure 1.2 is evident that at the LHC energies the probability of gluons to have the necessary momentum fraction is greatly increased. As as result, the primary contribution in $t\bar{t}$ production comes from gluon-gluon fusion. In fact, for the LHC 2010-2011 data-taking, the collision energy of $\sqrt{s} = 7$ TeV gives a $\sim 75\%$ contribution for $gg \to t\bar{t}$, at leading order, whereas for the nominal, $\sqrt{s}$ of 14 TeV, the contribution rises to $\sim 86\%$. Instead, for the Tevatron the most dominant production channel was via quark-antiquark annihilation with a contribution of approximately $\sim 91\%$. Figure 1.5 shows the leading-order Feynman diagrams of $t\bar{t}$ production, namely quark-antiquark annihilation ($q\bar{q} \to t\bar{t}$) and gluon-gluon fusion ($gg \to t\bar{t}$). It should be noted that at the next-to-leading order quark-gluon ($qg \to t\bar{t}$) contributions also appear.

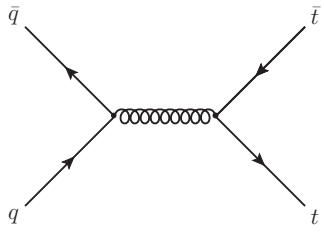

(a) Quark - antiquark annihilation.

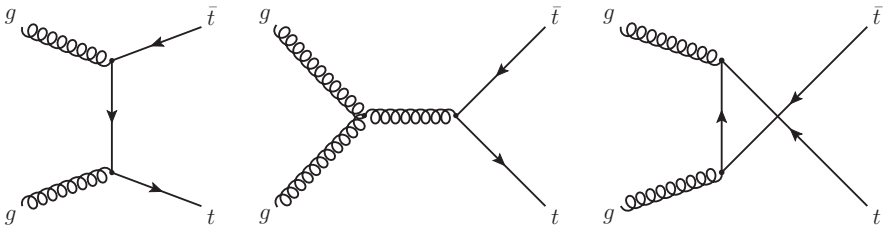

(b) Gluon-gluon fusion.

Figure 1.5: *The leading order diagrams for $t\bar{t}$ production.*

At the theoretical level, for estimating the top quark-pair production cross-section we can set the scale of the interaction to be equal to the mass of the top quark. As the top quark

mass is much larger than the QCD scale, the strong coupling constant will give a value of $\alpha_s(M_{top}) \sim 0.1$, thus allowing us to perform perturbation theory and estimate the short-distance cross-section. We can write the cross-section with the following form (stemming from expanding equation 1.2.2):

$$\hat{\sigma}_{t\bar{t}}(\hat{s}, M^2_{top}, \alpha_s(\mu^2), \mu^2) = \frac{\alpha_s^2(\mu^2)}{M^2_{top}} \mathcal{F}_{t\bar{t}}(\rho, M^2_{top}, \alpha_s(\mu^2), \mu^2) \ , \tag{1.3.4}$$

where $\hat{s} = x_1 x_2 s$, corresponding to the squared center-of-mass energy of the colliding partons, $\rho = 4M^2_{top}/\hat{s}$, and $\mathcal{F}_{t\bar{t}}$ is the perturbative series of dimensionless scaling functions which correspond to the order of calculation. It is therefore written as:

$$\mathcal{F}_{t\bar{t}}(\rho, M^2_{top}, \alpha_s(\mu^2), \mu^2) = \mathcal{F}^{(0)}_{t\bar{t}}(\rho) + 4\pi\alpha_s(\mu^2) \left[\mathcal{F}^{(1)}_{t\bar{t}}(\rho) + \overline{\mathcal{F}}^{(1)}_{t\bar{t}}(\rho) \ln \frac{\mu^2}{M^2_{top}} \right] + \mathcal{O}(\alpha_s^2) \ , \tag{1.3.5}$$

where the first term corresponds to the leading-order estimate, the second term to the next-to-leading order and so on. At each order, the necessary Feynman diagrams that contribute are taken into account and are integrated in the whole momentum phase-space. For leading-order the tree-level gluon-gluon fusion and quark-antiquark annihilation diagrams are important and the result is proportional to α_s^2.

One may assume that higher order corrections corrections are not necessary, given the small value of α_s, however, when considering the coefficients of those terms, significant contributions may arise. Moreover, as mentioned earlier, the dependence of the leading-order estimate from the renormalization/factorization scale is significant and with including higher order corrections we can reduce this effect. These highlight the importance of implementing higher order corrections. At the next-to-leading order ($\mathcal{O}(\alpha_s^3)$), both virtual and real contributions are taken into account. The virtual corrections arise from interference of the tree-level amplitude with one-loop virtual amplitudes, resulting in ultra-violet and infra-red divergencies. The ultra-violet divergencies are handled by the renormalization scheme while infra-red effects are eventually cancelled by the factorization. On the other hand, the real corrections appear from amplitudes due to flavor excitation, gluon splitting or direct gluon emissions. These, also give rise to contributions to the $t\bar{t}$ production cross-section from the qg and $g\overline{q}$ channels. In this case, soft (low-energy) or collinear effects may emerge which cannot be calculated with perturbation, instead they are isolated through factorization. Typical examples of next-to-leading order virtual and real corrections to $t\bar{t}$ production are shown in figure 1.6. It should be mentioned that the actual contribution of the $gg \to t\bar{t}$ channel rises at the next-to-leading order to $\sim 83\%$, for LHC collisions at $\sqrt{s} = 7$ TeV, and $\sim 90\%$ for the LHC at $\sqrt{s} = 14$ TeV, which is significantly higher than the leading-order expectation, thus emphasizing the need for higher-order corrections in the theoretical predictions.

An exact calculation at the next-to-next-to-leading order ($\mathcal{O}(\alpha_s^4)$) does not exist. Instead, approximate methods are applied where the appearing logarithmic terms at next-to-leading order, which result after factoring collinear divergencies into the PDFs, are re-summed to the perturbative expansion at a given α_s order. The most up-to-date theoretical cross-section estimate[9] for the inclusive $t\bar{t}$ production for proton-proton collisions at $\sqrt{s} = 7$ TeV is taken at this approximate next-to-next-to-leading order and is given at [54, 55]:

$$\sigma_{t\bar{t}} = 164.57^{+4.30}_{-9.27}(\text{scale})^{+7.15}_{-6.51}(\text{PDF}) \text{ pb.} \tag{1.3.6}$$

This calculation assumes a mass of $M_t = 172.5$ GeV and uses the `CTEQ6.6` next-to-leading order PDF [56]. For the analysis performed in this thesis these numbers are used as reference.

[9] Cross-sections are given in units of barn. 1 barn $= 10^{-28}$ m^2

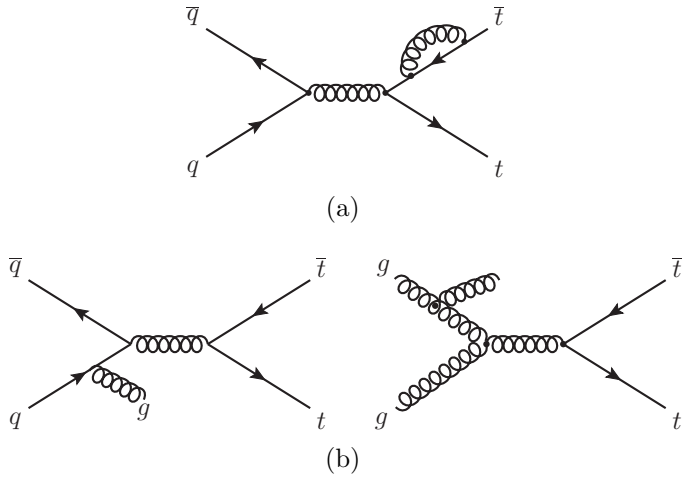

Figure 1.6: *Next-to-leading order ($\mathcal{O}(\alpha_s^3)$) virtual (a) and real (b) corrections to $t\bar{t}$ production in proton-proton collisions.*

1.3.2 Top quark final state topology

The top quark decays predominantly into a W boson and a b-quark, $t \to Wb$. The decay width of this process can be written at leading order in the following form [57]:

$$\Gamma_{LO}(t \to Wb) = \frac{G_F m_t^3}{8\pi\sqrt{2}} |V_{tb}|^2 \left(1 - \frac{M_W^2}{M_t^2}\right)^2 \left(1 + 2\frac{M_W^2}{M_t^2}\right) \ , \tag{1.3.7}$$

where G_F is the Fermi constant and $|V_{tb}|$ the CKM matrix element. Assuming three quark generations and unitarity of the CKM matrix, the value of the V_{tb} is found to be [53]:

$$V_{tb} = 0.999152^{+0.000030}_{-0.000045} \ , \tag{1.3.8}$$

which justifies the initial expectation, $\Gamma_{t\to Wb} \approx \Gamma_t$. After including higher order QCD corrections the decay width becomes:

$$\Gamma(t \to Wb) = \Gamma_{LO} \left[1 - \frac{2\alpha_s}{3\pi} f\left(y\right)\right] \ , \tag{1.3.9}$$

where the function $f(y)$ is defined as:

$$f(y) = \frac{2\pi^2}{3} - 2.5 - 3y + 4.5y^2 - 3^2 \ln y \ , \text{ and}$$
$$y = \frac{M_W^2}{M_t^2} \ .$$

Using $M_W = 80.4$ GeV and $M_t = 173$ GeV, we have $\Gamma_t = 1.34$ GeV which corresponds to a lifetime of roughly $5 \cdot 10^{-25}$ seconds [58]. This is the most striking characteristic of the top quark, since its lifetime is about an order of magnitude smaller than the hadronization timescale. As a result, it decays via the weak interaction long before it hadronizes and therefore its properties can be directly probed through its decay products.

The final topology of a $t\bar{t}$ event depends entirely on the decay of the W bosons. The W boson decays either leptonically, $W \to \ell\nu_\ell$, or hadronically, $W \to q\bar{q}'$. Naturally, this gives three distinct channels:

- The *di-leptonic* channel: when both W bosons decay leptonically, the final state consists of two high-p_{T} charge leptons and two high-p_{T} neutrinos, and two jets from b-quark hadronization (b-jets).
- The *single-lepton* channel: when one W boson decays leptonically and the other hadronically. The signal consists of one high-p_{T} charged lepton, its corresponding neutrino, the two b-jets and two jets from light-quark hadronization (light-jets).
- The *fully-hadronic* channel: when both W bosons decay hadronically. The signature consists exclusively of jets, namely the two b-jets and four light-jets.

The leptonically decaying W boson can result in any of the three flavors ($e\nu_e$, $\mu\nu_\mu$ or $\tau\nu_\tau$). The analysis presented in this thesis focuses on the single-lepton $t\bar{t}$ channel with an electron, $t\bar{t}(e)$, or a muon, $t\bar{t}(\mu)$, in their final state. The reason for making the distinction for the channels with τ-leptons in their final state, is because the τ decays fast, either hadronically ($\sim 65\%$) producing jets, or leptonically via $\tau \to e\nu_e\nu_\tau$ ($\sim 17.8\%$) or $\tau \to \mu\nu_\mu\nu_\tau$ ($\sim 17.2\%$). In the first case, it is difficult to distinguish the τ from a jet at the experimental level, while in the second case it is almost impossible to distinguish it from the original W boson decay. Figure 1.7 shows schematically the different decay channels of the $t\bar{t}$. The contributions, assuming a branching ratio for the hadronically decaying W boson of 67.6% [53], are 43.8% from single-lepton with about 1/3 having a τ-lepton in the final state, 10.5% from di-leptonic events with roughly half having at least one τ-lepton, and 45.7% are fully-hadronic decays.

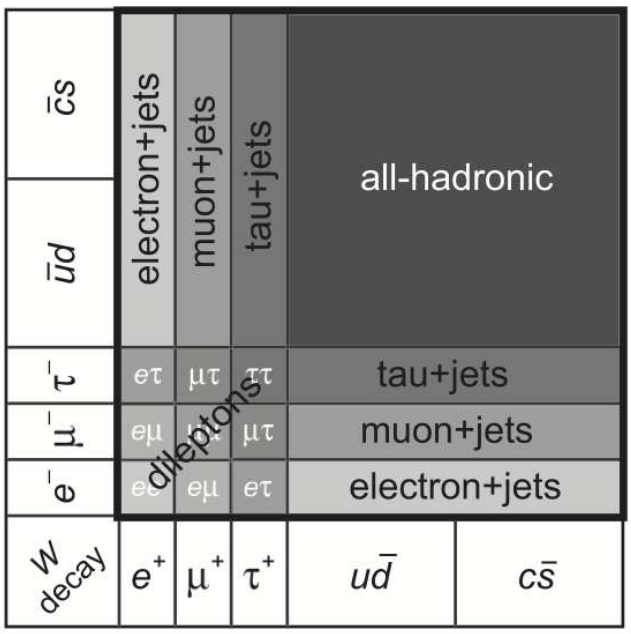

Figure 1.7: *Overview of the different decay channels of a $t\bar{t}$ event. Plot taken from [59].*

1.3.3 Backgrounds to single-lepton $t\bar{t}$ events

As discussed in the previous section, the single-lepton topology, that is of interest for this thesis, consists of a rather complex signature that involves a charged lepton, a neutrino and at least[10] four jets from which two are b-jets. Additionally, the charged lepton is expected

[10] If we consider the radiating effects, such as ISR/FSR, the final number of jet in the final state may be significantly higher than four.

to have a high-p_{T}, as it is the decay product of a massive object (W boson), but also be quite *isolated*, namely without much activity around its trajectory. Despite the distinctive characteristics of the single-lepton $t\bar{t}$ events, other processes may still resemble the final state of our *signal*[11]. These processes are typically the *background* and for the analysis we perform in this thesis the following are relevant:

- QCD multi-jet events[12].
- Events with a vector-boson (W or Z bosons) produced with associated jets.
- Single-top events.
- Diboson events.

We discuss each of these backgrounds in the next paragraphs.

QCD multi-jets

The LHC environment is swamped by the large background of QCD events having a total cross-section at the order of $\mathcal{O}(1mb)$. Most of these events are the result of $2 \to 2$ processes, such as $q\bar{q} \to gg$, $gg \to gg$, $qg \to qg$, where, due to hadronization, quarks and gluons result in energetic jets. Higher order processes ($2 \to 3, 4, 5$) are also very probable, resulting in higher jet multiplicities. In these cases, extra jets are produced from initial and final state radiation through parton branching; examples of such processes are shown in figure 1.8.

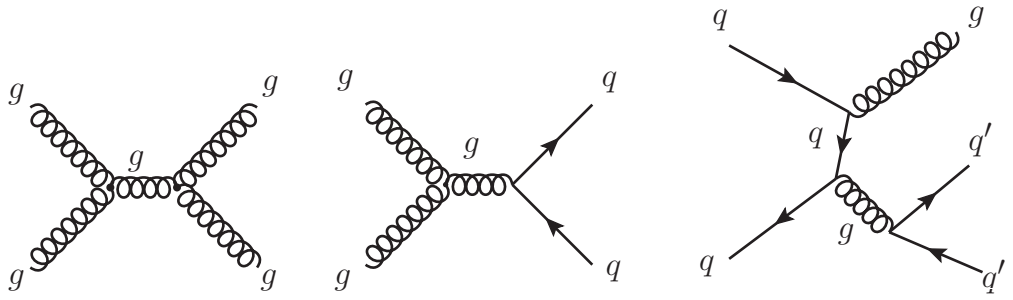

(a) QCD $2 \to 2$ (b) QCD $2 \to 3$

Figure 1.8: *Example Feynman diagrams for different QCD processes.*

For the QCD multi-jet events to be considered as background to the single-lepton $t\bar{t}$ channels, a lepton must be present while also the energy balance of the event must show significant missing energy due to the neutrino requirement. Experimentally, QCD events are considered as background only if the lepton, originating from decays inside the jets (non-prompt), passes the identification criteria that an analysis has set. Additionally, for the electron final state, a jet may be misidentified as an electron ('fake') increasing the probability for the event to be seen as signal. The overall probability for a QCD event to satisfy the necessary requirements is very small. However, this is balanced by the extremely large cross-section of the QCD multi-jet processes and therefore a significant fraction of events will still be mistaken as signal. Requiring the presence of b-jets further reduces the contribution of this background, however a considerable amount of QCD events still comes with associated heavy-quark production.

Theoretically, predicting the cross-section of QCD multi-jet processes is difficult. Although for typical di-jet $2 \to 2$ processes this is fairly simple, when considering leading-order $2 \to N$ processes (where $N > 2$) every extra outgoing parton must take into account an additional

[11] We will be using the term 'signal' to refer to the $t\bar{t}$ events of interest for this analysis.
[12] Hereafter called simply as QCD events.

factor of α_s. As the scale of the interaction is typically set to the scale of the produced particle or jet, for radiating partons this scale is at the limit of the perturbative region and therefore, unlike the $t\bar{t}$ production, the α_s is not small. Due to the strong scale dependence, the added uncertainty with every α_s factor is quite large and each outgoing parton further increases the uncertainty in the inclusive production cross-section. Including higher-order corrections can reduce this uncertainty, however, this is practically unfeasible. At leading order the $2 \to 2$ processes are described by no less than ten Feynman diagrams and when considering higher order corrections this number increases dramatically. In addition to the above, the low-energy showers and hadronization processes, that occur at certain stages of the above events, also introduce a significant uncertainty as they cannot be calculated exactly. Generally, the theoretical prediction on the normalization of QCD multi-jet events cannot be trusted a priori at the LHC and therefore it poses a great challenge for the related analyses.

Vector-boson production with associated jets

In high-energy hadron collisions, W and Z bosons can be produced directly from the hard-process via quark-antiquark annihilations. At the LHC, because the reaction involves only protons (uud), the process requires at least one sea-antiquark to emerge from the one colliding particle and interact with a quark from the other. For W boson production, a change of the third component of the weak isospin (T_3) happens with an up-type quark interacting with a down-type quark and the emitted boson has $T_3 = +1$ (for W^+) or $T_3 = -1$ (for W^-). Instead, the Z boson production does not involve a change of T_3, therefore both quarks have to be up-type or down-type and the resulting boson's T_3 is zero.

The W bosons decay to either a charged lepton and its neutrino (leptonic decay) or to a pair of an up-type and a down-type quark (hadronic decay). In approximately one-third of the times, the produced W boson will undergo a leptonic decay and often associated jets due to initial or final state radiation ($2 \to N$ processes) may emerge (W+jets). When the number of jets is sufficiently large, namely at least four jets are identified, these events constitute an important background for $t\bar{t}$ single-lepton decays. Naturally, if the performed analyses requires b-jets to be identified, the contribution is reduced significantly. However, W+jets events with associated heavy quark production ($b\bar{b}$, c or $c\bar{c}$) are also possible. Example Feynman diagrams of W+jets are shown in figure 1.9, the $W + 1$ parton is a clear example of a $2 \to 2$ process where in one case (left) one of the two quarks radiates a gluon before interacting with the other quark, while in the second case (right) a gluon is emitted from one of the protons and then splits into a quark-antiquark pair, and one of which interacts with the second incoming quark.

On the other hand, the Z bosons decay into a fermion and its anti-particle. Therefore, the final state may result into jets (hadronic) when decaying into quarks, into a pair of neutrinos (invisible) or into two charged leptons (leptonic). Similarly to W boson events, the Z boson events may also contain jets due to initial or final state radiation, including processes where heavy quarks are produced. However, due to the existence of the second charged lepton, their contribution as background to the single-lepton $t\bar{t}$ is not expected to be of significant amount as they can be vetoed easily with a multiplicity requirement.

For the same reasons as in the case of QCD multi-jet events, the prediction of the W+jets and Z+jets cross-sections becomes more difficult when extra outgoing partons are added. In fact, the precise next-to-leading order estimate of the W+4 jets and Z+4 jets productions at the LHC has only recently became available [60, 61]. At leading order the cross-sections of these processes have been estimated up to the order of six associated jets, naturally involving large uncertainties as in the case of the multi-jet events.

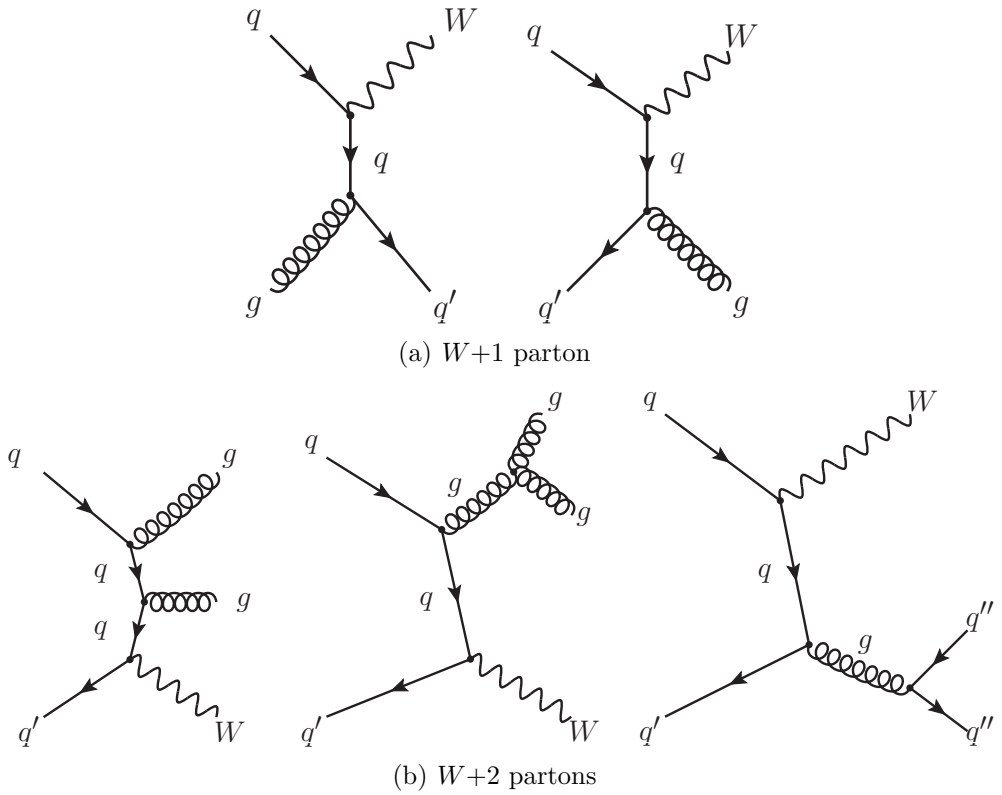

Figure 1.9: *Feynman diagrams for the W+1 parton with $qg \to Wq$ (a-left) and $q\bar{q} \to Wg$ (a-right), and W+2 parton processes.*

Single-top production

The production of single-top events was briefly introduced in section 1.3.1. The highest cross-section at the LHC comes from the t-channel with $\sigma_t = 64.2 \pm 2.6$ pb [62], while the Wt-channel gives a considerable contribution with $\sigma_{Wt} = 15.6 \pm 1.3$ pb[63]. The s-channel, on the other hand, has the smallest cross-section of all, $\sigma_s = 4.6 \pm 0.2$ pb [64]. In all of the cases, the cross-section is estimated theoretically at the approximate next-to-next-to-leading order.

The final state of all channels, when produced in association with jets, may easily resemble the signature of the signal events in many ways e.g. if the top quark results to a leptonic final state, or if the associated W decays leptonically and the top quark hadronically etc. However, the overall cross-section for this process is lower than the one of the $t\bar{t}$ signal and it only becomes a sizable background when requiring b-jet identification, which are present in this topology. Figure 1.10 shows example Feynman diagrams for each single-top production channel.

Diboson production

The vector-boson production in association with jets, that was presented earlier, referred to a single boson being produced. However, associated production of two bosons is also possible, namely with WW, WZ and ZZ. An example Feynman diagram is shown in figure 1.11. The production cross-section for these processes are in general quite low, when compared to the cross-section of signal events. In particular at next-to-leading order, the inclusive cross-sections are for the WW production, $\sigma_{WW} = 44.9$ pb, for the WZ production, $\sigma_{WZ} = 18.0$ pb and for the ZZ production channel only $\sigma_{ZZ} = 9.2$ pb [65].

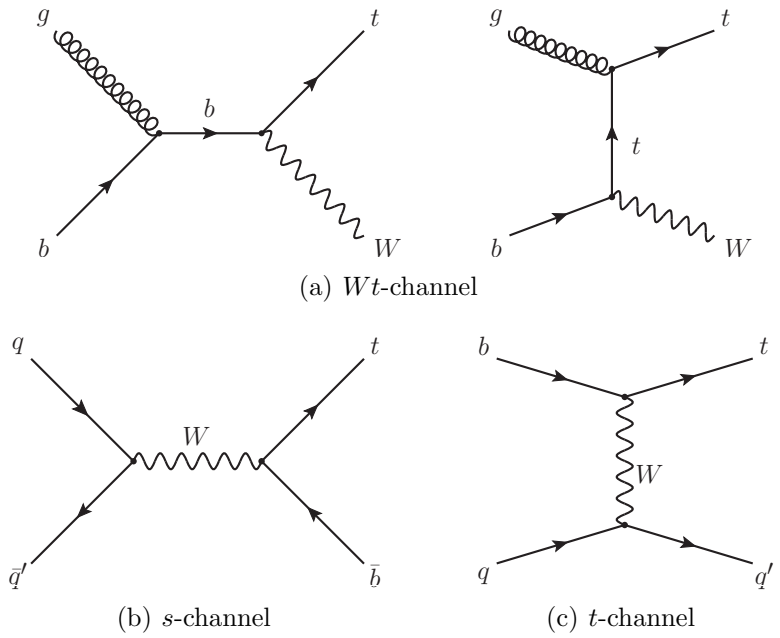

(a) Wt-channel

(b) s-channel

(c) t-channel

Figure 1.10: *The leading order single-top diagrams for the three different production channels.*

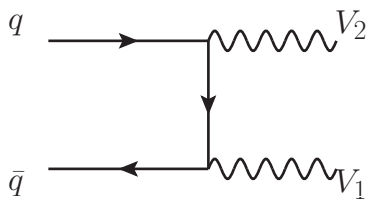

Figure 1.11: *An example of di-boson production where V stands for either W or Z bosons.*

1.3.4 Importance of top quark-pair cross-section measurement

Understanding the physics related with the top quark is of significant importance for the Standard Model. This argument is easily justified by simply considering equation 1.1.40 where, taking the experimentally measured values of the top quark mass and the vacuum expectation value for the Higgs field, the resulting coupling between the top quark and Higgs is close to unity. This indicates that the top quark may play an important role in the mechanism of electroweak symmetry breaking.

The first step in performing precise measurements of the properties of the top quark is to understand its production mechanism. As the LHC enters a previously unexplored energy region for particle physics, our current knowledge of QCD will be put to test. Therefore, it is necessary to establish that the theoretical and experimental agreement of the $t\bar{t}$ production cross-section estimate, initially shown at the Tevatron, also holds in this environment. Possible deviations from expectation may indicate the presence of physics that has not yet been observed. A particular example is the possibility of resonances in the $t\bar{t}$ system which are not expected by the Standard Model. Considering the nominal running parameters of the LHC, the expected rate of $t\bar{t}$ events is so greatly improved (approximately one $t\bar{t}$ pair per second) that the cross-section measurement not only is feasible but it can also be made with a great accuracy, thus being more sensitive to such new physics effects.

Except from establishing the validity of the production mechanisms of $t\bar{t}$ events at the LHC, an accurate cross-section determination lays the road to the measurement of many of the top quark's properties. The most striking example, which is also directly related with the search for the Higgs boson, is the measurement of the top quark mass which is directly related with the $t\bar{t}$ cross-section (see equation 1.3.4). Figure 1.12 shows this dependence, estimated at both next-to-leading and approximate next-to-next-to-leading orders for LHC at $\sqrt{s} = 14$ TeV.

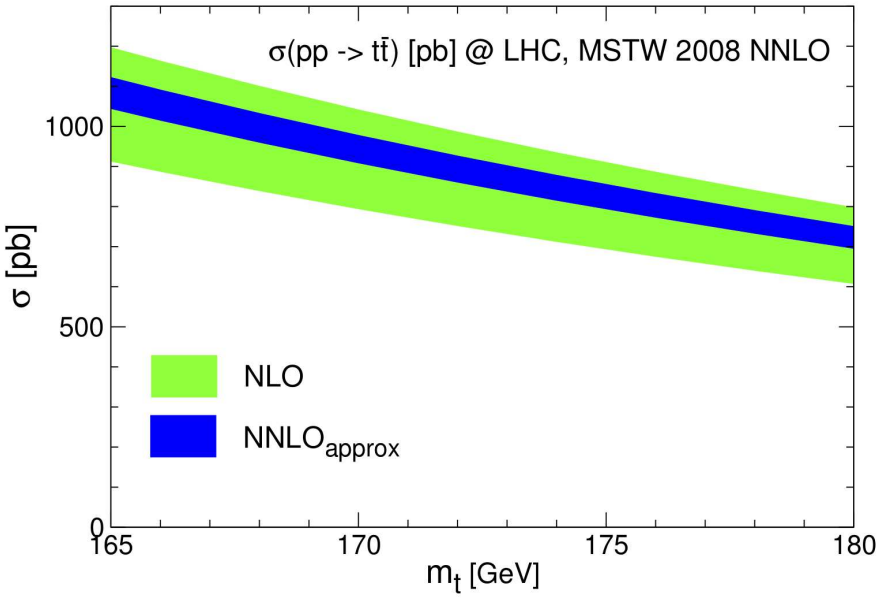

Figure 1.12: *Dependence of the top quarks cross-section from its mass at next-to-leading and the approximate next-to-next-to-leading order, estimated for proton-proton collisions at the LHC ($\sqrt{s} = 7$ TeV). The* `MSTW2008NLO` *is used as a PDF. Figure taken from [66].*

A precise determination of the top quark mass can provide, together with the measurement of the W mass, constraints on the mass of the Standard Model Higgs. This evident when considering radiative (one-loop) corrections in the Standard Model Lagrangian [67], in which case the mass term for the W boson (initially shown in equation 1.1.36) can be re-written in the following form:

$$M_W^2 = \frac{\alpha\pi}{\sqrt{2}G_F} \cdot \frac{1 + \Delta r/2}{\sin^2\theta_W} \ , \tag{1.3.10}$$

where G_F is the Fermi constant, α is the QED coupling constant, θ_W is the Weinberg angle, which can be written as $\sin^2\theta_W = 1 - M_W^2/M_Z^2$, and Δr corresponds to the radiative corrections applied. Using the measurements of the Z mass [68], the QED coupling constant [69] and the Fermi constant [70], the W mass is left to depend only on the radiative corrections. When considering the top quark loops, we have:

$$\Delta r_{top} \approx \frac{3G_F M_{top}^2}{8\sqrt{2}\pi^2 \tan^2\theta_W} \ , \tag{1.3.11}$$

which suggests a strong dependence between the mass of the W boson and the top quark. For the case of the Standard Model Higgs corrections, we have the following form:

$$\Delta r_{Higgs} \approx \frac{3G_F M_W^2}{8\sqrt{2}\pi^2} \left(\ln\frac{M_{Higgs}^2}{M_Z^2} - \frac{5}{6} \right) \ . \tag{1.3.12}$$

Clearly, from the relation between the masses of the top quark and the W boson, the mass of the Standard Model Higgs can be constrained. It should be noted however, that since the dependence between the W mass and the Higgs mass evolves logarithmically, only a loose constraint can be placed. Figure 1.13 shows the relationship between the three masses as estimated using direct (LEP2, Tevatron) and indirect (LEP1, SLD) measurements of the W and top quark masses.

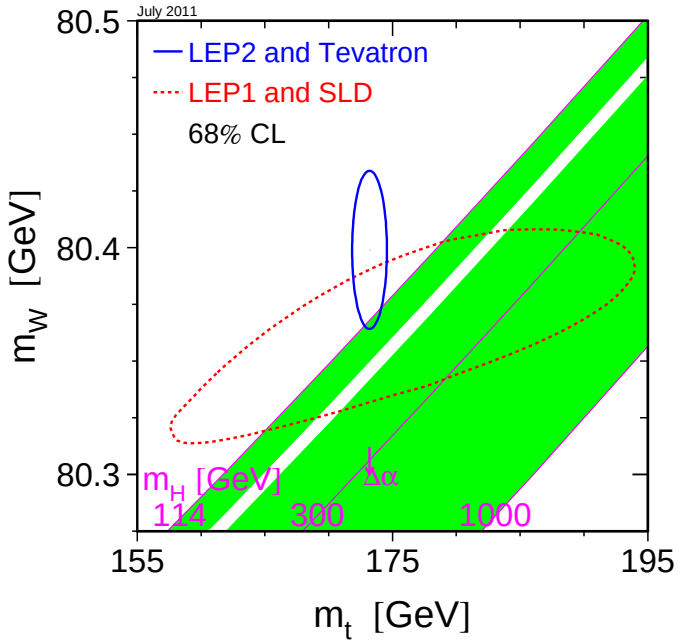

Figure 1.13: *Dependance between the W boson and the top quark mass and their relation with the Higgs mass. Contours shown at 68% confidence level. Figure taken from [71], version of summer 2011.*

Lastly, the $t\bar{t}$ events, and in particular the single-lepton final states, have a distinctive complex signature which involves the presence of a charged lepton, its neutrino and a high multiplicity of jets, including jets induced by b-quark. Effectively, for the detection of such events almost all detector parts, as will be shown in chapters 2, 3 and 4, are used. Therefore, a largely pure $t\bar{t}$ sample can effectively be used to commission and calibrate the experimental apparatus even from the beginning of the data-taking. The determination of cross-section naturally provides a road towards such sample.

1.4 Event generation and Monte Carlo samples

An important part of a physics analysis is the simulation of the processes that are expected to be observed. The software we use for this task, wrap the theoretical and experimental knowledge of the physics of interest and provide events randomly but within the allowed kinematic phase-space (*event generation*). Subsequently, generated events are interfaced with the simulation of the detector in order to provide a representation of a real physics signal. These are the Monte Carlo simulations and they allows us to perform feasibility studies, systematic studies and to a certain extend compare the theoretical expectations with the real data.

1.4.1 Generators

The various sub-processes which take place during a proton-proton collision have been briefly described in section 1.3.1. Certain generators are able to simulate the complete process from the initial interaction up to the hadronization and decay level. Other generators are more specialized in a certain process. Often a combination of different packages is used in order to improve the accuracy of the simulation. The general purpose generators that are used in this thesis are: `Pythia` [72], `Herwig` [73] and `Sherpa` [74]. The main specialized generators that are used are: `MCatNLO` [75, 76, 77, 78], `AcerMC` [79], `AlpGen` [80], `POWHEG` [81] and `Jimmy` [82].

Hard-process

The hard-process takes place at the high-Q^2 regime of the simulation, where perturbation theory can be applied. Taking into account all the contributing Feynman diagrams of a process, and at a certain order α_s, the simulation estimates the matrix element at each phase-space point. Subsequently, it integrates over the complete phase-space, taking into account possible cuts that might be applied, in order to determine the cross-section. Naturally, with including higher-order corrections, virtual and real, the simulation of the hard-process becomes more challenging. All but the `Jimmy` generator can perform matrix element calculations, while the rest are described in the following:

- *`Pythia`* and *`Herwig`*: Both of these general purpose generators contain a large number of built-in processes which are generated at the lowest QCD order, therefore they are at fixed leading-order. However, they provide reduced accuracy in multi-parton final states as they handle QCD and QED radiations only at the parton shower evolution (see next paragraphs). Therefore, they are not the primary choice for the generation of events. In the analysis presented here `Herwig` is used only for the generation of di-boson events.
- *`AlpGen`*: The `AlpGen` generator is a leading-order matrix element generator specialized for multi-parton final states ($2 \to N$). In contrast to `Pythia` and `Herwig`, it provides a more accurate description by using perturbation theory on all the relevant tree-level Feynman diagrams with a fixed number of outgoing partons. The result is bare partons and therefore an additional simulation package must be interfaced to handle subsequent processes. This generator is used to simulate the background W+jets, Z+jets and QCD multi-jet processes up to five outgoing partons.
- *`Sherpa`*: Similarly to `AlpGen` it provides a more accurate description of multi-parton final states based on matrix element calculation. However, it can also handle internally the rest of the processes without needing to couple with an external package. In this thesis, W+jets events generated with this generator are used for systematic studies.
- *`AcerMC`*: Also a leading-order generator, the `AcerMC` provides a library of matrix-element calculation of a number of built-in processes. Primarily aimed for background processes with a large number of partons in the final state, such as W+jets and Z+jets, it can also be used for the simulation of $t\bar{t}$ events. Simulated $t\bar{t}$ events using `AcerMC` are used for the systematic studies of ISR/FSR effects.
- *`MCatNLO and POWHEG`*: The only generators in this thesis that provide both real and virtual corrections in the generation process at next-to-leading order. Primarily used for the production of top quark events. The `MCatNLO` is used to generate the signal events for the $t\bar{t}$ cross-section analysis, while `POWHEG` is used for systematic studies. The `MCatNLO` is also used for generation of the single-top events.

Parton shower

The parton shower is the process which describes the splitting of the partons, namely ISR and FSR effects. These interaction evolve at lower Q^2 and until the hadronization effects take over. For the leading-order matrix element generators including these processes implies practically a correction to higher-order calculation. However, since these calculations involve also collinear ($\theta_{qg} \downarrow 0$) and low-energy ($E_g \downarrow$) effects they cannot be handled by the matrix element as they lead to infinities. Most leading-order generators use leading-order DGLAP splitting functions [83, 84, 85, 86] with Sudakov form factors [87] to include these regimes.

Underlying event

Description of the underlying event in simulations is distinct from the ISR/FSR effects as it mainly involves the proton remnants. These processes are semi-hard with low-transverse momentum and evolve mainly in the forward directions. However, they affect also the hard-process due to color connection. It is not unlikely that jets from the underlying event are present in more central region and in the vicinity of the hard-process products. Generators describe this process as a $2 \to 2$ QCD interaction. The underlying event can be described by both `Pythia` and `Herwig` packages although the latter is usually interfaced with `Jimmy` which is dedicated for this task.

Hadronization

At the hadronization scale perturbative calculations cannot be followed anymore. Instead generators model the related physics to produce results and then tune these models with respect to the observed data. In this thesis, the generator mainly implement the two following models: the *cluster fragmentation* and the *string fragmentation*. The cluster fragmentation splits all gluon into $q\bar{q}$ pairs and forms neutral color clusters from the available quarks. The cluster subsequently decay into lighter clusters of hadrons. On the other hand, the string fragmentation 'sees' field lines between color charges. With increasing distance between quark-antiquark pairs the potential energy of the field increases and causes new quarks to emerge. Hadrons are formed from the available quarks. In this view, gluons are seen as kinks which in the end affect the angular distribution of the hadrons.

For the MC samples in our analysis, almost all use the `Herwig` package for the hadronization. Alternatively, `Pythia` is used together with the `AcerMC` generator and the `POWHEG` generator for parton shower systematic studies on the signal sample.

Decay

The decay process takes over after the hadronization step. Generators simply use experimental data, namely branching ratios, to determine the final state of the events. All particles with a decay length below 10mm are allowed to decay, while the rest are treated in the detector simulation.

Matrix element to parton shower matching

Combining the matrix element result with the parton showers simulation has the consequence of double counting. This is because the same Feynman diagram can describe both a higher order matrix element calculation for an e.g. $2 \to 3$ event, and an matrix element calculation of the same process $2 \to 2$ but where the parton shower splits an outgoing gluon to emit a soft or collinear parton. Even though the two processes occur at different energy scales they may still give overlap kinematically. The goal then becomes clear that a specific separation point

must be given which will define up to which level the processes are handled by the matrix element while leaving the rest for the parton shower scheme.

The AlpGen generator, which is used for most background processes, implements such a matching method named MLM [88, 89]. With this procedure, the jets produced from the parton shower are matched to the matrix element partons. Naturally, an algorithm which reconstructs the hadronized partons is required. The matching is simply done based on the distance between the jet and the parton in the pseudo-rapidity (η) versus azimuthal angle (ϕ) space. If every hard parton is matched to a jet the event is kept, otherwise it is rejected.

1.4.2 Monte Carlo samples

A large number of Monte Carlo samples were used for the analysis presented hereafter. This section provides some details on certain technical aspects that are of interest.

Top-quark samples

Both the top quark pair sample (signal) and the single-top use the MCatNLO generator (v3.41) with the CTEQ6.6 PDFs [56]. The top quark mass, for all cases, is taken to be 172.5 GeV which is accordance with the current world average. The $t\bar{t}$ sample is inclusive for the leptonic states, namely containing both single-lepton and di-lepton events in all flavors. A distinct, but with the same generation parameters, sample is used for the fully-hadronic $t\bar{t}$ events. On the other hand, the single-top processes are produced exclusively for each of the three channels. For the Wt-channel an overlap removal scheme is applied [90] to avoid double counting with $t\bar{t}$ final states. These diagrams happen on higher order correction of the Wt-channel and can effectively be interpreted as $t\bar{t}$ at leading-order with a decay of the anti-quark into a Wb pair. In all cases, the Herwig and Jimmy combination is used for the parton shower, hadronization and underlying event processes.

Also, as mentioned earlier, the POWHEG samples are used for the systematic checks. These are produced with both Herwig and Pythia for the hadronization process in order to accommodate relevant systematic studies. Lastly, the AcerMC leading-order samples, interfaced with Pythia for hadronization, are used in order to estimate the ISR/FSR systematic uncertainty.

W+jets and Z+jets samples

As mentioned in the previous section, the vector-boson samples are generated using the AlpGen (v2.13) package with the CTEQ6L1 PDF [91], while their hadronization and underlying event physics is handled by Herwig and Jimmy. For the MLM matching the minimum p_{T} that is used to define the parton shower jet is 20 GeV, every jet below that value is not considered for the matching. Also, the matching distance is set to be 0.7. For the W+jets samples, four individual processes are used: the W+light jets, the $Wb\bar{b}$+jets, the $Wc\bar{c}$+jets and the $Wc(\bar{c})$+jets. The W+light jets sample has a significant overlap with the other three samples and therefore, an appropriate removal of the duplicate events is performed. The Z+jets events are not considered in their full phase-space but are restricted to the region where $M_{\ell^+\ell^-} > 40$ GeV.

QCD multi-jet samples

The QCD multi-jet samples use the same configuration as the W+jets samples. However, in order to facilitate their production and usage for the $t\bar{t}$ analysis certain requirements are placed. The following apply for these samples:

- **QCD Slicing:** The samples are separated into transverse momentum slices and each event is categorized according to the highest jet p_{T}(leading-jet). The jets are considered at the truth level, namely after applying a reconstruction algorithm on the stable particles after hadronization of the event. With this classification, the lowest leading-jet threshold available in the simulation is $p_T^{leading} \geq 17$ GeV, thus any event with leading-jet p_{T} lower than that value is not saved.
- **QCD Filtering:** For the lower p_{T} slices, which contain all events with leading-jet p_{T} of less than 140 GeV, the true cross-section is very large and it is practically difficult to generate enough events that correspond to a reasonable integrated luminosity. Therefore, filters are applied that register only events which are likely to pass the requirement of the nominal $t\bar{t}$ analysis. For analyses that look at the leptonic decay channels, and specifically the ones where a muon or an electron exists in the final state, two filters are used for QCD events with increased probability of passing the default cuts. The muon filter which requires all events to contain a true muon with $p_{\mathrm{T}} \geq 10$ GeV and $|\eta| \leq 2.8$, and the jet filter where all events must have at least three jets with $p_{\mathrm{T}} \geq 25$ GeV and at least one more jet with $p_{\mathrm{T}} \geq 17$ GeV , with all jets within $|\eta| \leq 5.0$. The muon filtered samples are, typically, used for the analysis with $t\bar{t}$ events with a muon in the final state, while the jet-filtered sample is used when an electron exists in the $t\bar{t}$ final state.

1.5 Summary

We introduced in this chapter the theoretical context upon which we base our cross-section measurement. The implementation of the Standard Model has been very successful in the past decades providing physicists with an important predictive tool. The most striking example is the prediction and subsequent discovery of the vector bosons, W and Z, as a result of the unification of the electromagnetic and the weak force and the imposition of the Higgs mechanism as the means for them to gain mass. In addition, the categorization of the elementary particles into generations, although not fully understood, led to the discovery of the top quark, a milestone for modern physics.

The top quark was also presented. Measuring the cross-section of the top quark pair production is an important first goal for the experiments at the LHC. The measurement provides an excellent first test for QCD and for the first time at the energy regimes that the LHC explores; deviations may surely give a hint for the existence of new physics. In addition, the cross-section measurement opens up the door for precision measurements of the different top quark's properties. In the following chapters, we present one of the first $t\bar{t}$ cross-section measurements performed with the ATLAS detector using the very first collision data delivered by the LHC.